



Tube dynamics and low energy Earth–Moon transfers in the 4-body system

Kaori Onozaki^a, Hiroaki Yoshimura^{a,*}, Shane D. Ross^b

^a Department of Applied Mechanics and Aerospace Engineering, Waseda University, 3-4-1, Okubo, Shinjuku, Tokyo 169-8555, Japan

^b Engineering Mechanics Program, Virginia Tech, 495 Old Turner Street, Blacksburg, VA 24061, USA

Received 26 January 2017; received in revised form 20 July 2017; accepted 31 July 2017

Available online 8 August 2017

Abstract

In this paper, we show a low energy Earth–Moon transfer in the context of the Sun–Earth–Moon–spacecraft 4-body system. We consider the 4-body system as the coupled system of the Sun–Earth–spacecraft 3-body system perturbed by the Moon (which we call the Moon-perturbed system) and the Earth–Moon–spacecraft 3-body system perturbed by the Sun (which we call the Sun-perturbed system). In both perturbed systems, analogs of the stable and unstable manifolds are computed numerically by using the notion of Lagrangian coherent structures, wherein the stable and unstable manifolds play the role of separating orbits into transit and non-transit orbits. We obtain a family of non-transit orbits departing from a low Earth orbit in the Moon-perturbed system, and a family of transit orbits arriving into a low lunar orbit in the Sun-perturbed system. Finally, we show that we can construct a low energy transfer from the Earth to the Moon by choosing appropriate trajectories from both families and patching these trajectories with a maneuver.

© 2017 COSPAR. Published by Elsevier Ltd. All rights reserved.

Keywords: Low energy transfer; 4-body system; Perturbed system; Tube dynamics; Lagrangian coherent structures; Astrodynamics

1. Introduction

In designing trajectories for space missions, reducing the energy required, in other words, the fuel, is an important issue. A long-standing focus of much attention is the problem of designing spacecraft trajectories from the Earth to the Moon. Typically, the patched conic approximation has been used to design such transfer trajectories, in which the Earth–Moon–spacecraft(S/C) 3-body system is modeled approximately as the Earth–S/C and Moon–S/C 2-body systems. However, it is known that trajectories designed with the patched conic approximation may require excessive amounts of energy in transferring to the Moon and also that the resulting trajectory may not be

accurate enough for the transfer design (e.g., Bate et al., 1971). Belbruno and Miller (1993) developed a low energy spacecraft trajectory by considering the Sun's gravitational effect as a perturbation to the gravitational effects due to the Earth and the Moon. The concept of a *Weak Stability Boundary* (WSB), which is a transition region between gravitational capture by and escape from a planet (Belbruno, 1987), was used to construct the lower energy transfer to the Moon. The transfer was implemented in the Japanese Hiten Mission in 1991. Later, another Hiten-like trajectory was developed by Koon et al. (2001) in the context of the *coupled planar circular restricted 3-body system*, in which the Sun–Earth–Moon–S/C 4-body system can be modeled approximately by the coupled system of the Sun–Earth–S/C and Earth–Moon–S/C 3-body systems. In particular, they employed so-called *tube dynamics*, in which stable and unstable manifolds of cylindrical topology separate transit and non-transit orbits to

* Corresponding author.

E-mail addresses: green-11street@uri.waseda.jp (K. Onozaki), yoshimura@waseda.jp (H. Yoshimura), sdross@vt.edu (S.D. Ross).

construct arbitrary trajectories. Mingotti et al. (2009) implemented low-thrust propulsion within the framework of the coupled 3-body system to design a low energy Earth–Moon transfer, and obtained an optimal transfer in the 4-body system using the Earth–Moon transfer constructed in the coupled 3-body system as the first candidate. A low-energy transfer in a system using body ephemerides was constructed by Parker (2009), which used the stable manifold and a similar procedure to the coupled 3-body system proposed by Parker (2006). Subsequently, Onozaki et al. (2016a) developed a systematic design method for the 4-body system by extending the concept of the coupled 3-body system: The Sun–Earth–Moon–S/C system was regarded as the coupled system of the Sun–Earth–S/C system with the Moon’s perturbation (hereinafter referred to as the *Moon-perturbed system*) and the Earth–Moon–S/C system with the Sun’s perturbation (hereinafter referred to as the *Sun-perturbed system*), which was referred to as the *coupled 3-body system with perturbations*.

On the other hand, for various practical reasons related to the design of low energy trajectories, we require boundary conditions such that the spacecraft departs from a Low Earth Orbit (LEO) and arrives into a Low Lunar Orbit (LLO). In this situation, we seek an optimal trajectory among the possible trajectories subject to these boundary conditions. Topputo (2013) numerically obtained a global set of optimal solutions for the boundary conditions in the 4-body system by using direct transcription and multiple shooting, and related the solutions with previously proposed transfers. Onozaki et al. (2016b) showed that there exists an optimal trajectory for the coupled 3-body system in the sense that no ΔV is required to patch the trajectories between the Sun–Earth–S/C and the Earth–Moon–S/C systems.

Now, we also note recent developments in the theory of (hyperbolic) *Lagrangian Coherent Structures* (LCS), which were proposed by Haller (2001). The LCS indicate separation structures typified by stable and unstable manifolds, as a computational tool for detection of the invariant manifolds (and their analogs) in non-autonomous systems such as a 4-body system. Shadden et al. (2005) elaborated a theory of LCS wherein they are defined as ridges of Finite Time Lyapunov Exponent (FTLE) field and illustrated the computation of LCS by some examples of two-dimensional fluids. In contrast, Haller (2011) proposed a variational theory of LCS in terms of the Cauchy–Green strain tensor, since the ridges of FTLE fields may lead to false positives and false negatives in the detection of LCS. Farazmand and Haller (2012) showed the computation of LCS based on the variational theory. An extension to elliptic LCS and 3-dimensional flows was made by Blazeviski and Haller (2014). For applications to astrodynamics, it was shown by Gawlik et al. (2009) that LCS from the ridges of FTLE fields can be computed in a 4-dimensional phase space for the non-autonomous planar elliptic restricted 3-body system. Similar computations of

the LCS for the circular 3-body system were made by Onozaki and Yoshimura (2014) and Short and Howell (2014) and others. Short and Howell (2014) also demonstrated the computation in the 4-body and ephemeris systems. Oshima and Yanao (2014) investigated the gravity assists concerned with the LCS for 4-body systems. A false positive for the ridges of the FTLE field due to a primary mass was investigated by Pérez et al. (2012). Further developments relevant to the LCS were made; for instance, Short et al. (2015) applied eigenvectors of the Cauchy–Green tensor to flow control segments to effectively find a connecting condition of trajectories. Pérez et al. (2015) developed another detection tool of the separation structures by using the Jet Transport which indicates the image after the advection of the neighbor set around an initial point by a flow.

In this paper, we present the design of a low energy transfer from the Earth to the Moon by using the coupled 3-body system with perturbations for modeling the restricted 4-body system under the planar assumption. In particular, we consider a low energy trajectory subject to the boundary conditions that the spacecraft departs from a LEO and arrives into a LLO. In Section 2, we briefly review the Planar Circular Restricted 3-Body System (PCR3BS) in the context of tube dynamics. In Section 3, we derive the equations of motion of the planar bicircular restricted 4-body system with respect to two different rotating frames together with a coordinate transformation. In Section 4, the tubes (i.e., the stable and unstable manifolds of the perturbed systems) are obtained by numerically extracting the LCS from the FTLE field. Then, we demonstrate how the obtained LCS separates orbits. In Section 5, a trajectory design from the LEO to the LLO is shown in the framework of the coupled 3-body system with perturbations. Using the characteristics of the tube structures, we obtain the family of trajectories that depart from the LEO and the family of those that arrive into the LLO. Finally we show how a low energy Earth–Moon transfer can be constructed by choosing an appropriate orbit from each family such that the required ΔV is minimized under given conditions.

2. Planar circular restricted 3-body system

2.1. Mathematical model

We begin this section with a brief review of the dynamics of the PCR3BS that is used to analyze the motion of a spacecraft subject to the gravitational pull of two masses. In this paper, we focus upon the planar case, in which we assume that the two masses move at constant angular velocity on the same plane in circles around their common mass center, and also that the spacecraft of a negligible mass moves in the same plane, as shown in Fig. 1. Let m_1 and m_2 ($m_2 < m_1$) be the primary and secondary masses, respectively. Choose the unit of mass as $m_1 + m_2$ and the unit of length as the distance between the primary and secondary masses. The unit of time is set so that the orbital

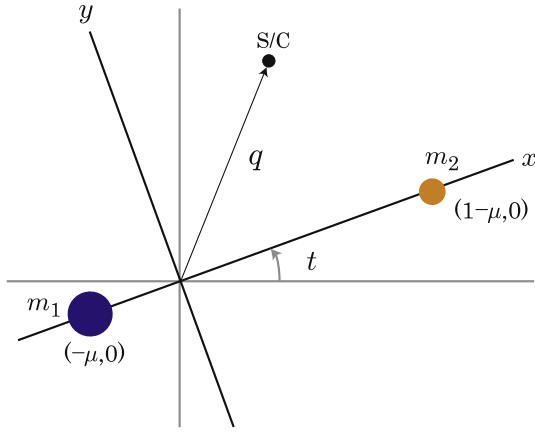


Fig. 1. PCR3BS.

period of masses becomes 2π . Then, the system becomes nondimensional with the gravitational constant G set to unity. Let $q = (x, y)^\top \in Q = \mathbb{R}^2$ be the position of the spacecraft in the frame that rotates with the masses, and denote by $\dot{q} = dq/dt = (v_x, v_y)^\top \in T_qQ \cong \mathbb{R}^2$ the velocity with respect to the nondimensional time t . In the above, $Q = \mathbb{R}^2$ denotes the configuration space and $TQ = \mathbb{R}^2 \times \mathbb{R}^2$ the velocity phase space (the tangent bundle) of Q . Introducing the mass parameter by $\mu = m_2/(m_1 + m_2)$, as in Szebehely (1967) and Koon et al. (2011), the equation of motion in the rotating frame is

$$\ddot{q} - 2\tilde{\Omega}\dot{q} - q = -\frac{(1-\mu)}{|q-q_1|^3}(q-q_1) - \frac{\mu}{|q-q_2|^3}(q-q_2), \tag{1}$$

where

$$\tilde{\Omega} = \begin{pmatrix} 0 & 1 \\ -1 & 0 \end{pmatrix}.$$

In the above, $q_1 = (-\mu, 0)^\top$ and $q_2 = (1-\mu, 0)^\top$ indicate the positions of the primary and secondary masses, respectively. The energy of the spacecraft is given by the sum of the kinetic energy and the effective potential consisting of the centrifugal and gravitational potentials as

$$E(q, \dot{q}) = \frac{1}{2}|\dot{q}|^2 - \frac{1}{2}|q|^2 - \frac{1-\mu}{|q-q_1|} - \frac{\mu}{|q-q_2|},$$

which is preserved along the solution curves of the PCR3BS. For the Sun–Earth–S/C system, the mass parameter is $\mu = m_E/(m_S + m_E) \cong 3.02319 \times 10^{-6}$, and for the Earth–Moon–S/C system the mass parameter is $\mu = m_M/(m_E + m_M) \cong 1.21536 \times 10^{-2}$.

2.2. Invariant manifolds and tubes

It follows from Eq. (1) that there exist the three Lagrange points (L_1, L_2, L_3) on the x axis together with the equilateral triangle points (L_4, L_5) . Setting the energy

E to some constant value E_0 , we can define an energy surface $\mathcal{E} \subset TQ$ as

$$\mathcal{E}(\mu, E_0) = \{w = (x, y, v_x, v_y) \in TQ | E(x, y, v_x, v_y) = E_0\}.$$

Letting $\tau : TQ \rightarrow Q; (x, y, v_x, v_y) \mapsto (x, y)$ be the tangent bundle projection, one can define Hill’s region by projecting the energy surface $\mathcal{E}(\mu, E_0)$ onto Q such that $\tau(\mathcal{E}(\mu, E_0)) \subset Q$. The forbidden region in which the spacecraft energy does not permit its motion is thus defined as the region excluding Hill’s region from the configuration space. In this paper, we choose an energy E_0 slightly greater than the energy at L_2 so that the spacecraft passes near L_1 and L_2 , as shown in Fig. 2.

The collinear Lagrange points (L_1, L_2, L_3) are unstable saddle \times center equilibrium points. If the energy level is fixed consistent with E_0 , then unstable periodic orbits, called *Lyapunov orbits*, exist around both L_1 and L_2 . One can obtain the stable and unstable manifolds associated with the Lyapunov orbits, which are homeomorphic to $S^1 \times \mathbb{R}$ and hence are called *tubes*. Hill’s region can be divided into five regions by vertical lines (parallel to the y -axis). Sets of two lines are on the right- and left-hand sides of each Lyapunov orbit, as depicted by the dashed lines in Fig. 2. Then, two *neck* regions are defined as the regions that are bounded by each set of vertical lines and include L_1 or L_2 . The other regions, excluding the neck regions, are classified as the P_1 region including the primary mass, the P_2 region including the secondary mass, and the X region outside the P_1 and P_2 regions. Here we introduce the notation $W_{i,A}^s$ for the stable manifolds that asymptotically approach the Lyapunov orbit around $L_i, (i = 1, 2)$ from the $A(= P_1, P_2, X)$ region and $W_{i,A}^u$ for the unstable manifolds that depart a Lyapunov orbit around $L_i, (i = 1, 2)$ toward the $A(= P_1, P_2, X)$ region. In Fig. 2, the Lyapunov are shown in orange, whereas the stable and unstable manifolds orbits projected onto the x - y plane in light-green and red, respectively.

The manifold tubes separate orbits into *transit* and *non-transit orbits* (e.g., Conley, 1968; Koon et al., 2011). Namely, an orbit inside the tubes is a transit orbit. For example, if a spacecraft is inside the tube in some region,

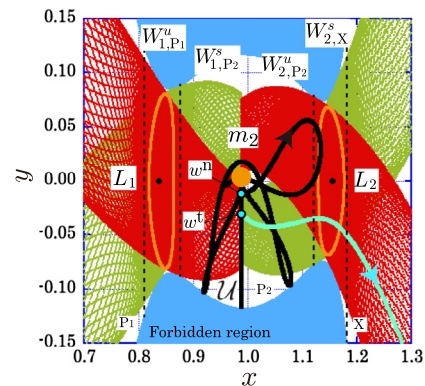


Fig. 2. Flow around the secondary mass.

it is transported to another region through a neck region. On the other hand, an orbit existing outside the tubes is a non-transit orbit, where a spacecraft in a region remains in the same region or returns to the same region through a neck region. For the rest of this paper, we do not specifically mention the transportation through a neck region.

In Fig. 2, we show that a Poincaré section $\mathcal{U} \subset \mathcal{E}(\mu, E_0)$ is set to detect the tubes on the 2-dimensional space given by

$$\mathcal{U} := \{w = (x, y, v_x, v_y) \in \mathcal{E}(\mu, E_0) \mid x = 1 - \mu, y < 0, v_x > 0\}.$$

Define the j -th intersection of the stable manifold $W_{i,A}^s$ ($i = 1, 2$ and $A = P_1, P_2, X$) with \mathcal{U} by $\Gamma_{i,A}^{j,s} = W_{i,A}^s \cap \mathcal{U}$ and also define by $\Gamma_{i,A}^{j,u} = W_{i,A}^u \cap \mathcal{U}$ the j -th intersection of the unstable manifold $W_{i,A}^u$ ($i = 1, 2$ and $A = P_1, P_2, X$). We illustrate $\Gamma_{2,P_2}^{1,s}$ in Fig. 3 and choose points w^t inside $\Gamma_{2,P_2}^{1,s}$ and w^n outside $\Gamma_{2,P_2}^{1,s}$. The transit orbit from the P_2 region to the X region integrated from w^t and the non-transit orbit staying in the P_2 region from w^n are colored cyan and black, respectively, as shown in Fig. 2.

3. Bicircular model for the planar restricted 4-body system

We consider the bicircular model (Huang, 1960; Simó et al., 1995) for the restricted Sun–Earth–Moon–S/C 4-body system as illustrated in Fig. 4, where the Sun and the barycenter of the Earth and the Moon (Earth–Moon barycenter) rotate on the circular orbits around the center of mass (CM) of the whole system. The distance between the Sun and the Earth–Moon barycenter is given by $a_S \cong 1.49598 \times 10^8$ km and the angular velocity of the Sun and the barycenter is denoted by $\omega_S \cong 1.99640 \times 10^{-7}$ rad/s. The Earth and the Moon rotate on the circular orbits around their barycenter with the angular velocity $\omega_M \cong 2.66498 \times 10^{-6}$ rad/s, and the distance between the Earth and the Moon is $a_M \cong 3.84400 \times 10^5$ km. The masses of the Sun, the Earth and the Moon are $m_S \cong 1.99976 \times 10^{30}$ kg, $m_E \cong 5.97219 \times 10^{24}$ kg and $m_M \cong 7.34767 \times 10^{22}$ kg, respec-

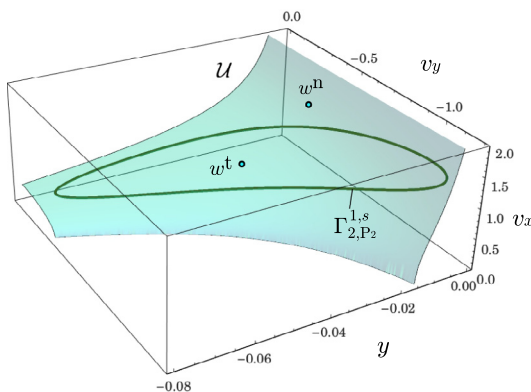


Fig. 3. First intersection of the stable manifold W_{2,P_2}^s with \mathcal{U} .

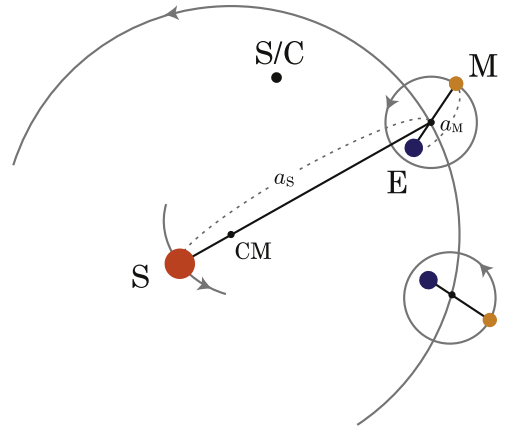


Fig. 4. Bicircular model.

tively. We assume that the spacecraft and the planets move on the same plane.

We will show that this bicircular model of the restricted 4-body system can be regarded as two different perturbed 3-body systems by splitting the motion of the spacecraft into mathematical models described in two different rotating frames.

3.1. Moon-perturbed system and the S– B_{EM} rotating frame

We normalize the system quantities by choosing the mass unit as $m_S + m_E + m_M$, the length unit as a_S , and the time unit as $T_S = 2\pi/\omega_S$ such that the gravitational constant G is unity. We define the mass parameters by $\mu_S = (m_E + m_M)/(m_S + m_E + m_M) = 3.02319 \times 10^{-6}$ and $\mu_M = m_M/(m_E + m_M) = 1.21536 \times 10^{-2}$. By this normalization, the distance between the Earth and the Moon becomes $\alpha_M = a_M/a_S$. The angular velocity of the system of the Earth and the Moon is selected to be $\varpi_M = \omega_M/\omega_S$. Denoting the normalized time by \bar{t} , the angle with respect to the line connecting the Sun and the Earth–Moon barycenter is given by $\bar{\theta}_M = (\varpi_M - 1)\bar{t} + \bar{\theta}_{M0}$, where $\bar{\theta}_{M0}$ indicates an initial value of $\bar{\theta}_M(\bar{t})$. As shown in Fig. 5, we set a local coordinate system that rotates with the Sun and the Earth–Moon barycenter, which we shall refer to as the S– B_{EM} rotating frame.

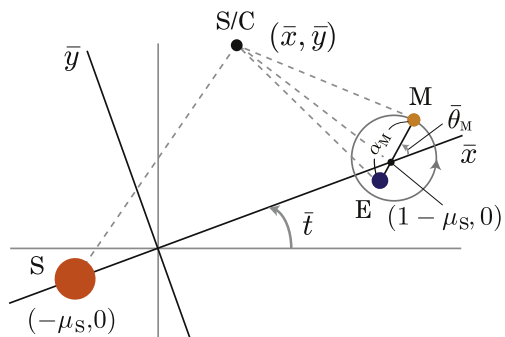


Fig. 5. Bicircular model in the S– B_{EM} rotating frame.

Denoting by $\bar{q} = (\bar{x}, \bar{y})^\top \in Q$ the position of the spacecraft in the S–B_{EM} rotating frame and by $\bar{q}' = d\bar{q}/d\bar{t} = (\bar{v}_x, \bar{v}_y)^\top \in T_{\bar{q}}Q$ the velocity, the equation of motion of the spacecraft in the S–B_{EM} rotating frame is given by

$$\bar{q}'' - 2\tilde{\Omega}\bar{q}' - \bar{q} = -\frac{(1 - \mu_S)}{|\bar{q} - \bar{q}_S|^3}(\bar{q} - \bar{q}_S) - \frac{\mu_S(1 - \mu_M)}{|\bar{q} - \bar{q}_E|^3}(\bar{q} - \bar{q}_E) - \frac{\mu_S\mu_M}{|\bar{q} - \bar{q}_M|^3}(\bar{q} - \bar{q}_M), \quad (2)$$

where the positions of the Sun, the Earth and the Moon are indicated by

$$\begin{aligned} \bar{q}_S &= (-\mu_S, 0)^\top, \\ \bar{q}_E &= ((1 - \mu_S) - \alpha_M\mu_M \cos(\bar{\theta}_M), -\alpha_M\mu_M \sin(\bar{\theta}_M))^\top, \\ \bar{q}_M &= ((1 - \mu_S) + \alpha_M(1 - \mu_M) \cos(\bar{\theta}_M), \alpha_M(1 - \mu_M) \sin(\bar{\theta}_M))^\top, \end{aligned}$$

respectively.

The energy in the S–B_{EM} rotating frame is defined by

$$\bar{E}^{SE} = \frac{1}{2}|\bar{q}'|^2 - \frac{1}{2}|\bar{q}|^2 - \frac{(1 - \mu_S)}{|\bar{q} - \bar{q}_S|} - \frac{\mu_S(1 - \mu_M)}{|\bar{q} - \bar{q}_E|} - \frac{\mu_S\mu_M}{|\bar{q} - \bar{q}_M|}. \quad (3)$$

Note that this energy is *not* conserved along a solution curve because the system is non-autonomous.

If $\mu_M = 0$, (i.e., the Moon is neglected), then Eq. (2) coincides with the equation of motion of the Sun–Earth–S/C 3-body system. Therefore, the bicircular model can be considered as the Sun–Earth–S/C system perturbed by the Moon. In this paper, we refer to the bicircular model in the S–B_{EM} rotating frame as the *Moon-perturbed system*.

3.2. Sun-perturbed system and the E–M rotating frame

Now we revisit the bicircular model by introducing the E–M rotating frame, i.e., the local coordinate system rotating with the Earth and the Moon as shown in Fig. 6. Choosing the mass unit as $m_E + m_M$, the length unit as a_M , and the time unit as $T_M = 2\pi/\omega_M$, the gravitational constant G becomes unity. Then, the distance between

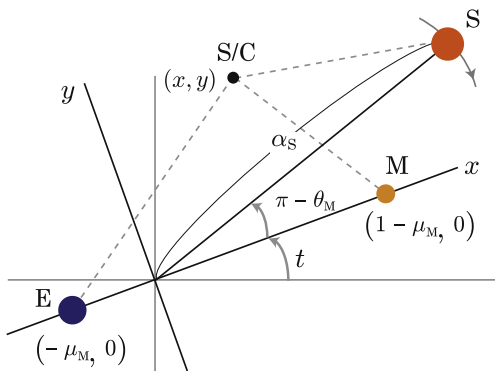


Fig. 6. Bicircular model in the E–M rotating frame.

the Sun and the Earth–Moon barycenter becomes $\alpha_S = a_S/a_M$ and the angular velocity of the system of the Sun and the barycenter can be described as $\varpi_S = \omega_S/\omega_M$. Note that $\alpha_S = \alpha_M^{-1}$ and $\varpi_S = \varpi_M^{-1}$.

Let $t \in I = [t_0 - T, t_0 + T] \subset \mathbb{R}$ be the time in the E–M rotating frame, where t_0 denotes the origin of the time interval (which is usually set to zero) and $T > 0$ denotes a certain time interval. Then the relative angle between the masses is given by $\theta_M(t) = (1 - \varpi_S)t + \theta_{M0}$. Denoting by $q = (x, y)^\top \in Q$ the position of the spacecraft in the E–M rotating frame and $\dot{q} = dq/dt = (v_x, v_y)^\top \in T_qQ$, the equation of motion in the E–M rotating frame is obtained as

$$\ddot{q} - 2\tilde{\Omega}\dot{q} - q = -\frac{1 - \mu_M}{|q - q_E|^3}(q - q_E) - \frac{\mu_M}{|q - q_M|^3}(q - q_M) - \frac{1 - \mu_S}{\mu_S|q - q_S|^3}(q - q_S) - \frac{1 - \mu_S}{\mu_S\alpha_S^3}q_S, \quad (4)$$

where q_S, q_E , and q_M indicate the position vectors of the Sun, the Earth, and the Moon, respectively, and are given by

$$\begin{aligned} q_S &= (-\alpha_S \cos(\theta_M), \alpha_S \sin(\theta_M))^\top, \\ q_E &= (-\mu_M, 0)^\top, \\ q_M &= (1 - \mu_M, 0)^\top. \end{aligned}$$

We define the energy in the E–M rotating frame (Simó et al., 1995) by

$$\begin{aligned} E^{EM} &= \frac{1}{2}|\dot{q}|^2 - \frac{1}{2}|q|^2 - \frac{1 - \mu_M}{|q - q_E|} - \frac{\mu_M}{|q - q_M|} - \frac{1 - \mu_S}{\mu_S|q - q_S|} \\ &\quad + \frac{1 - \mu_S}{\mu_S\alpha_S^3}\langle q_S, q \rangle, \end{aligned}$$

which is not conserved along a trajectory.

If we choose $\mu_S = 1$ (i.e., the Sun is neglected), then Eq. (4) is the equation of motion of the Earth–Moon–S/C system. Thus, we can consider the bicircular model in the E–M rotating frame as the Earth–Moon–S/C system perturbed by the Sun, which we shall refer to as the *Sun-perturbed system* (see also Qi et al., 2012).

3.3. Coordinate transformation

Now we show the coordinate transformation between the Moon-perturbed system and the Sun-perturbed system. The transformation of time is given by

$$\bar{t} = \frac{\omega_S}{\omega_M}t = \varpi_S t.$$

The transformation of the position vectors is

$$\bar{q} = \bar{q}_B + \frac{a_M}{a_S}C(t)q = \bar{q}_B + \frac{1}{\alpha_S}C(t)q, \quad (5)$$

where $\bar{q}_B = (1 - \mu_S, 0)^\top$ denotes the position of the Earth–Moon barycenter in the S–B_{EM} rotating frame and $C(t)$ is a rotation matrix given by

$$C(t) = \begin{pmatrix} \cos \theta_M(t) & -\sin \theta_M(t) \\ \sin \theta_M(t) & \cos \theta_M(t) \end{pmatrix}.$$

The velocity transformation is obtained by differentiating Eq. (5). The coordinate transformation for the velocity phase space, $\tilde{\varphi}: TQ \times I \rightarrow TQ \times I, (x, y, v_x, v_y, t) \mapsto (\bar{x}, \bar{y}, \bar{v}_x, \bar{v}_y, \bar{t})$, is given by

$$\bar{q}' = \frac{1}{\alpha_S \varpi_S} C(t) (\dot{q} - (1 - \varpi_S) \tilde{\Omega} q).$$

4. Tube dynamics in the perturbed systems

In a perturbed 3-body system (i.e., either the Moon-perturbed system or the Sun-perturbed system), a torus, which may be close to a periodic orbit (i.e., a nearly periodic orbit), exists instead of the periodic Lyapunov orbit of the PCR3BS. However, we expect that there will still be analogs of stable and unstable manifolds of the torus which will act as separatrices between transit and non-transit orbits, similar to the PCR3BS. Thus, we numerically demonstrate this separation by using the LCS concept, where an LCS approximates the generalized notion of invariant manifolds of time-dependent systems. Note that although the stable and unstable manifolds vary with time, these manifolds are invariant in a system eliminated time dependency by a transformation. Thus, we described these manifolds as the invariant manifolds.

In this paper, we compute the LCS as the ridges of FTLE fields (Shadden et al., 2005). The LCS may include false positives as described by Haller (2011), Pérez et al. (2012), while we extract the objective LCS from the innermost local maximum of FTLE fields by assuming that the intersection of the stable and unstable manifolds with a Poincaré section is homeomorphic to a circle.

4.1. Finite time Lyapunov exponents

To detect an LCS, we need to compute FTLE, which indicates the expansion ratio of the distance between two close points at some time and their distance after being advected by a vector field for some duration. We refer to Shadden et al. (2005) and Tallapragada and Ross (2013) for the definition of the FTLE.

Let D be an open subset of a phase space $M \subset \mathbb{R}^n$ and $w = (w_1, \dots, w_n)$ be an element of D . Consider a time-dependent dynamical system

$$\begin{cases} \dot{w}(t; t_0, w_0) = f(w(t; t_0, w_0), t), \\ w(t_0; t_0, w_0) = w_0, \end{cases}$$

where $w(t; t_0, w_0)$ is a smooth solution curve starting at an initial point $w_0 \in D$ at time t_0 and $f(w, t)$ is a given

time-dependent vector field. Then, the point w_0 moves to another point after a finite time interval T by the flow map:

$$\phi_{t_0}^{t_0+T}: D \rightarrow D; \quad w_0 \mapsto \phi_{t_0}^{t_0+T}(w_0) = w(t_0 + T; t_0, w_0).$$

The FTLE denotes a finite time average of the maximum expansion or contraction rate during the time interval T for a pair of neighboring phase space points at the initial time t_0 under advection by the flow map. Now, consider an infinitesimal perturbation δw_0 for the point w_0 . After the time interval T , the perturbation denoted by δw_T is

$$\begin{aligned} \delta w_T &= \phi_{t_0}^{t_0+T}(w_0 + \delta w_0) - \phi_{t_0}^{t_0+T}(w_0) \\ &= \left. \frac{d\phi_{t_0}^{t_0+T}(w)}{dw} \right|_{w=w_0} \delta w_0 + O(\|\delta w_0\|^2), \end{aligned}$$

where the matrix $d\phi_{t_0}^{t_0+T}(w)/dw$ is called the state transition matrix. By neglecting the higher-order terms $O(\|\delta w_0\|^2)$, the magnitude of the perturbation becomes

$$\|\delta w_T\| = \sqrt{\delta w_0, \Delta \delta w_0},$$

where Δ is a symmetric matrix given by

$$\Delta = \left(\left. \frac{d\phi_{t_0}^{t_0+T}(w)}{dw} \right|_{w=w_0} \right)^\top \left. \frac{d\phi_{t_0}^{t_0+T}(w)}{dw} \right|_{w=w_0}.$$

This is a finite time version of the (right) Cauchy-Green tensor.

The maximum stretching occurs when δw_0 is chosen so that it is aligned with the eigenvector of the maximum eigenvalue of Δ , which we denote by $\lambda_{\max}(\Delta)$. Let δw_0 be an initial perturbation aligned with the eigenvector, and it follows that

$$\max_{\delta w_0} \|\delta w_T\| = \sqrt{\lambda_{\max}(\Delta)} \|\delta w_0\|.$$

The FTLE field $\sigma_{t_0}^{t_0+T}: D \subset M \rightarrow \mathbb{R}$ associated with a finite time T is defined by

$$\sigma_{t_0}^{t_0+T}(w_0) = \frac{1}{|T|} \ln \sqrt{\lambda_{\max}(\Delta)}. \tag{6}$$

In this paper, we choose $t_0 = 0$ to compute the FTLE field for the 4-body system, denoted as σ^T . In order to compute the FTLE, following Tallapragada and Ross (2008), Gawlik et al. (2009), Ross et al. (2010), we set a regularly spaced rectilinear grid of tracers in a n -dimensional phase space to advect the grid of tracers forward in time by the fixed time T employing the Runge-Kutta-Fehlberg integrator, as in Press et al. (1992). To compute the FTLE numerically, we need to discretize $\frac{d\phi_{t_0}^{t_0+T}(w)}{dw}$ of Eq. (6) at each grid point by the central difference approximation as

$$\frac{\partial [\phi_{t_0}^{t_0+T}(w)]_i}{\partial w_j} \approx \frac{[\phi_{t_0}^{t_0+T}(w_1, \dots, w_j + \Delta w_j, \dots, w_n)]_i - [\phi_{t_0}^{t_0+T}(w_1, \dots, w_j - \Delta w_j, \dots, w_n)]_i}{2\Delta w_j},$$

where w_j and $[\phi_{t_0}^{t_0+T}(w)]_i$ are components of w and $\phi_{t_0}^{t_0+T}(w)$, respectively. The discrete size Δw_j is chosen so that the estimated truncation error of the matrix is smaller than the chosen acceptable error $\epsilon_{TOL} = 10^{-7}$. Regarding the estimation of the error, see [Appendix A](#).

4.2. Lagrangian coherent structures

We recall the definition of an LCS as proposed by [Shadden et al. \(2005\)](#), in which an LCS is defined by *ridges* of the FTLE field $\sigma^T(w)$. More formally, there exist two different but similar definitions of the LCS, namely, it is defined as a curvature ridge or a second-derivative ridge of σ^T , while the second-derivative ridge is identical to or a subset of the curvature ridge with local extrema of the FTLE field. In this paper, we employ the definition of the second-derivative ridge known as a simpler and convenient one as follows. First, the Hessian of the FTLE field is given by

$$\Sigma = \frac{d^2\sigma^T(w)}{dw^2}.$$

An LCS is defined as the second-derivative ridge of σ^T , which is given by an injective curve $c : (a, b) \rightarrow D$ that satisfies, for each s , the following conditions:

1. The vector $c'(s)$ is parallel to $\nabla\sigma^T(c(s))$.
2. $\Sigma(n, n) = \min_{\|u\|=1} \Sigma(u, u) < 0$ is required, where n is a unit normal vector to $c(s)$ and Σ is regarded as a bilinear form evaluated at each point $c(s)$.

A ridge of the backward-time FTLE field, which one can obtain by the negative integration time T , is called the *attracting LCS* that corresponds to the time-dependent analog of the unstable manifold. A ridge of the forward-time FTLE field with the positive integration time T is the *repelling LCS* that corresponds to the stable manifold. Note that, in this study, the integral time T is chosen sufficiently long so that the particular LCS exists stationary.

4.3. FTLE field and LCS in the Moon-perturbed system

Here, we investigate the stable manifold, (i.e., the repelling LCS), associated with the Lyapunov orbit of the Moon-perturbed system. To do this, we define an instantaneous energy surface at $\bar{t} = \bar{t}_0$ in the Moon-perturbed system by

$$\bar{\mathcal{E}}(\mu, \bar{E}_{\bar{t}_0}^{SE}) = \{\bar{w} = (\bar{x}, \bar{y}, \bar{v}_x, \bar{v}_y) \in TQ | \bar{E}^{SE}(\bar{x}, \bar{y}, \bar{v}_x, \bar{v}_y, \bar{t}_0) = \bar{E}_{\bar{t}_0}^{SE}\}.$$

In the above, $\mu = (\mu_S, \mu_M)$ and $\bar{E}_{\bar{t}_0}^{SE}$ denotes a fixed value for the energy at $\bar{t} = \bar{t}_0$ in the Moon-perturbed system.

Define a subspace $\bar{\mathcal{U}} \subset \bar{\mathcal{E}}(\mu, \bar{E}_{\bar{t}_0}^{SE})$ at $\bar{t} = \bar{t}_0$ in the Moon-perturbed system by

$$\bar{\mathcal{U}}(\mu, \bar{E}_{\bar{t}_0}^{SE}) := \{\bar{w} = (\bar{x}, \bar{y}, \bar{v}_x, \bar{v}_y) \in \bar{\mathcal{E}}(\mu, \bar{E}_{\bar{t}_0}^{SE}) \mid \bar{\theta}_M = 0, \bar{x} < 1 - \mu_S, \bar{y} = 0, \bar{v}_y < 0\}. \tag{7}$$

In order to see the FTLE field on the \bar{x} - \bar{v}_x -plane, we can locally introduce a projection

$$\pi : (\bar{x}, \bar{y}, \bar{v}_x, \bar{v}_y) \mapsto (\bar{x}, \bar{v}_x).$$

We show the FTLE field for the energy $\bar{E}_{\bar{t}_0}^{SE} = -1.5004$ in [Fig. 7](#) by setting a 1000×1000 grid within $(\bar{x}, \bar{v}_x) \in [0.993, 1] \times [-0.03, 0.03]$ on the Poincaré section $\bar{U}_0 := \pi(\bar{\mathcal{U}})$ and the integral time $T = 7$. We do not compute the collision points inside the Earth's surface 6371 km, namely, $|\bar{q} - \bar{q}_E| < 4.25875 \times 10^{-5}$; these points are colored in black in [Fig. 7](#). The overflow or underflow points caused by the separations due to the Moon in the FTLE computations are also colored in black. The instantaneous forbidden region is colored in white.

Here, recall from [Section 2.2](#) that the notations $\bar{\Gamma}_{2,E}^{i,s}$ and $\bar{\Gamma}_{1,E}^{i,s}$ denote the i -th intersection of the stable manifolds $\bar{W}_{2,E}^s$ and $\bar{W}_{1,E}^s$, respectively, with the subspace $\bar{\mathcal{U}}$. Namely, $\bar{\Gamma}_{2,E}^{1,s}$ denotes the subset $\bar{W}_{2,E}^s \cap \bar{\mathcal{U}}$ for the first intersection of $\bar{W}_{2,E}^s$ and $\bar{\mathcal{U}}$, which is the stable manifold toward the E region associated with the Lyapunov orbit \bar{L}_2 on $\bar{\mathcal{U}}$. Note that we use the same notation $\bar{W}_{2,E}^s$ and $\bar{\Gamma}_{2,E}^{1,s}$ to describe the stable manifold and the subset $\bar{W}_{2,E}^s \cap \bar{\mathcal{U}}$ as those for the Sun-Earth-S/C 3-body system in [Onozaki and Yoshimura \(2014\)](#).

[Fig. 7](#) shows some ridges that may correspond to several intersections $\bar{\Gamma}_{2,E}^{i,s}$ and $\bar{\Gamma}_{1,E}^{i,s}$ in [Onozaki and Yoshimura \(2014\)](#) and may also represent a separation that originates from the Moon. Moreover, we assume that the subset $\bar{\Gamma}_{2,E}^{1,s}$ is homeomorphic to a circle.

To detect the repelling LCS corresponding to $\bar{\Gamma}_{2,E}^{1,s}$ in the Moon-perturbed system, let us introduce the line l_φ on \bar{U}_0 at $\bar{\varphi} \in [0, 2\pi]$ defined by

$$l_\varphi = \{(\bar{x}, \bar{v}_x) \in \bar{U}_0 \mid \bar{x} = \bar{x}_c + r \cos \bar{\varphi}, \bar{v}_x = \bar{v}_{x_c} + r \sin \bar{\varphi}, r \in [0, r_{\max}] \subset \mathbb{R}\},$$

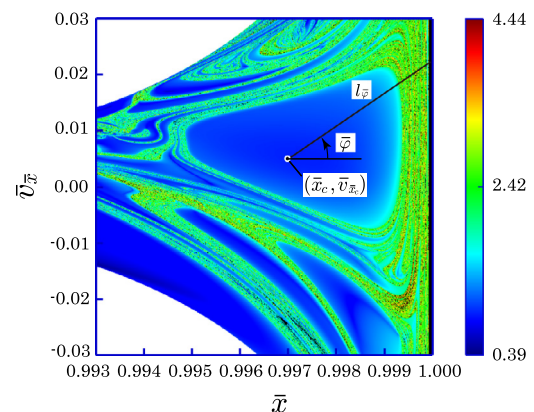


Fig. 7. FTLE field in the Moon-perturbed system ($T = 7$).

where $r_{\max} = 0.00009/\sqrt{(0.03 \cos \bar{\varphi})^2 + (0.003 \sin \bar{\varphi})^2}$ and $(\bar{x}_c, \bar{v}_{\bar{x}_c}) = (0.997, 0.005)$ is a point properly chosen in \bar{U}_0 . In order to extract the LCS on \bar{U}_0 , we compute the values of the FTLE on the line as illustrated in Fig. 8.

The repelling LCS may be obtained as the innermost local maximum of the FTLE as in Fig. 8. The computation of the FTLE and the extraction of the innermost ridge are iterated as needed by subsampling the grid. We show the LCS at each $\bar{\varphi}$ in Fig. 9. Set $\bar{w}^l = (\bar{x}, \bar{y}, \bar{v}_x, \bar{v}_y) = (0.999368, 0, 0.005, -0.0958139)$ on the LCS as the initial point at \bar{t}_0 . Thus we obtain a trajectory that approaches the Lyapunov-like orbit around \bar{L}_2 by forward integration for \bar{w}^l as shown in Fig. 10.

We also illustrate the cases in which the initial points are given by:

$$\begin{aligned} \bar{w}^t &= (\bar{x}, \bar{y}, \bar{v}_x, \bar{v}_y) = (0.999, 0, 0.005, -0.0732899), \\ \bar{w}^n &= (\bar{x}, \bar{y}, \bar{v}_x, \bar{v}_y) = (0.9998, 0, 0.005, -0.187686), \end{aligned}$$

where \bar{w}^t and \bar{w}^n are points located inside and outside the LCS, respectively. In Fig. 10, the obtained trajectories are shown to be transit and non-transit orbits associated with \bar{w}^t and \bar{w}^n , respectively.

Similarly, we can compute the repelling LCS for other instantaneous energies $\bar{E}_{t_0}^{SE}$.

4.4. FTLE field and LCS in the Sun-perturbed system

Let us compute the attracting LCS corresponding to the unstable manifold $W_{2,X}^u$ in the Sun-perturbed system. We use similar notation $W_{2,X}^u$ for the unstable manifold in the Sun-perturbed system as in the Moon-perturbed system and we make use of local coordinates $(x, y, v_x, v_y, t) \in TQ \times \mathbb{R}$ in the E-M rotating frame for all the computations. First, define an instantaneous energy surface $\mathcal{E}(\mu, E_{t_0}^{EM}) \subset TQ$ at $t = t_0$ in the E-M rotating frame by

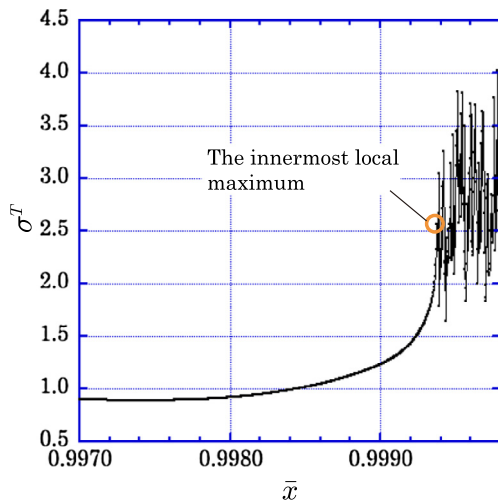


Fig. 8. FTLE on the line l_0 in the Moon-perturbed system ($T = 7$).

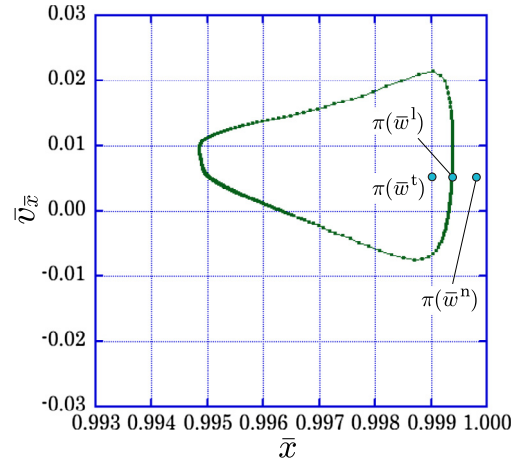


Fig. 9. Repelling LCS on \bar{U}_0 in the Moon-perturbed system ($T = 7$).

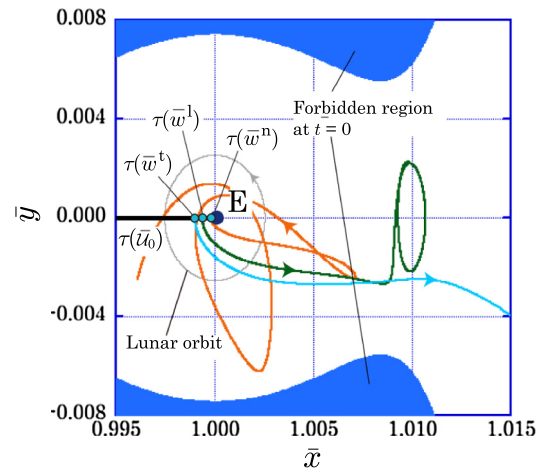


Fig. 10. Transit and non-transit orbits in the Moon-perturbed system.

$$\mathcal{E}(\mu, E_{t_0}^{EM}) = \{w = (x, y, v_x, v_y) \in TQ | E^{EM}(x, y, v_x, v_y, t_0) = E_{t_0}^{EM}\},$$

where $E_{t_0}^{EM}$ denotes a fixed value of the energy at $t = t_0$ in the E-M rotating frame, which is chosen so that the Hill's region at $t = t_0$ has a neck-like region. We define a subspace $\mathcal{U} \subset \mathcal{E}(\mu, E_{t_0}^{EM})$ at $t = t_0$ in the Sun-perturbed system by

$$\begin{aligned} \mathcal{U}(\mu, E_{t_0}^{EM}) &:= \{w = (x, y, v_x, v_y) \in \mathcal{E}(\mu, E_{t_0}^{EM}) \mid \\ \theta_M &= 2.55, x < 1 - \mu_M, y = 0, v_y < 0\}. \end{aligned} \tag{8}$$

Setting a rectilinear 1000×1000 grid within $(x, v_x) \in [0.91, 0.99] \times [-0.5, 0.2]$ on the Poincaré section $U_0 := \pi(\mathcal{U})$, the FTLE field on U_0 for $E_{t_0}^{EM} = -851.53$ and $T = -7$ is illustrated in Fig. 11. The instantaneous forbidden region is colored in white. We do not compute the collision points inside the Moon's surface 1737.5 km , namely, $|q - q_M| < 4.52003 \times 10^{-3}$; these points are colored in black in Fig. 11. We can assume that the ridges

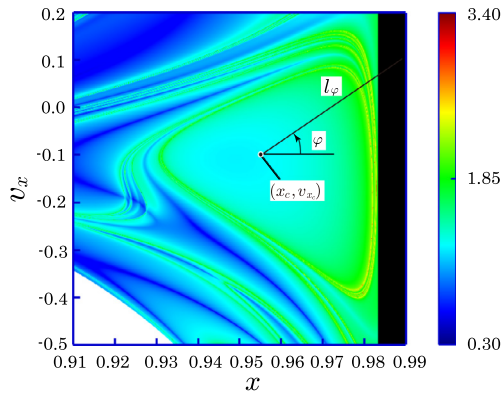


Fig. 11. FTLE field on U_0 in the Sun-perturbed system ($T = -7$).

in the FTLE field correspond to the i -th intersections of the unstable manifolds defined by $\Gamma_{1,M}^{i,u} = W_{1,M}^u \cap \mathcal{U}$ and $\Gamma_{2,M}^{i,u} = W_{2,M}^u \cap \mathcal{U}$.

As before, to extract the $\Gamma_{2,M}^{1,u}$ we set the line

$$l_\varphi = \{(x, v_x) \in U_0 \mid x = x_c + r \cos \varphi, \\ v_x = v_{xc} + r \sin \varphi, r \in [0, r_{\max}]\},$$

where $r_{\max} = 0.014 / \sqrt{(0.4 \cos \varphi)^2 + (0.035 \sin \varphi)^2}$ and $(x_c, v_{xc}) = (0.955, -0.1) \in U_0$. The attracting LCS on U_0 corresponding to the subset $\Gamma_{2,M}^{1,u}$ can be computed as the innermost local maximum of the FTLE on the line l_φ . The computation and extraction are iterated, as in Section 4.3 by subsampling the grid. We show the FTLE on l_0 in Fig. 12 and the extracted LCS in Fig. 13.

Setting the initial points $w^1 = (x, y, v_x, v_y) = (0.981683, 0, -0.1, -1.92901) \in TQ$ on the LCS, the integrated orbit is shown in Fig. 14. The orbit seems to be asymptotic to a Lyapunov-like orbit in backward-time. If we choose the initial points inside and outside the LCS as

$$w^t = (x, y, v_x, v_y) = (0.975, 0, -0.1, -1.29225), \\ w^n = (x, y, v_x, v_y) = (0.985, 0, -0.1, -2.88393),$$

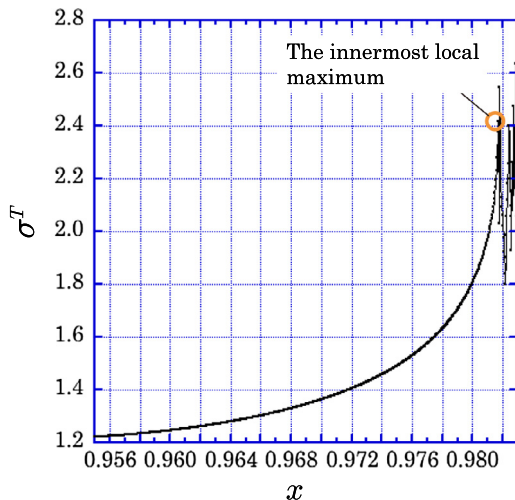


Fig. 12. FTLE on l_0 in the Sun-perturbed system ($T = -7$).

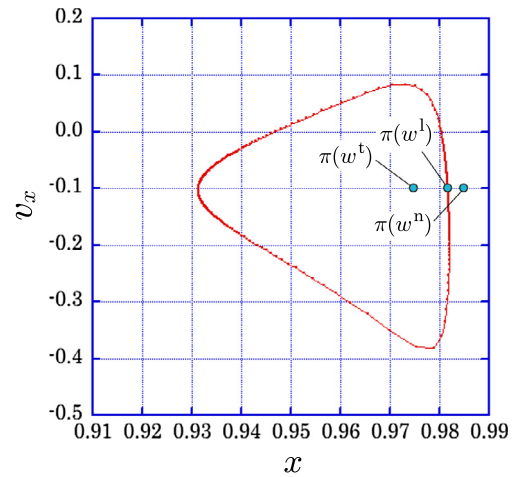


Fig. 13. Attracting LCS on U_0 in the Sun-perturbed system ($T = -7$).

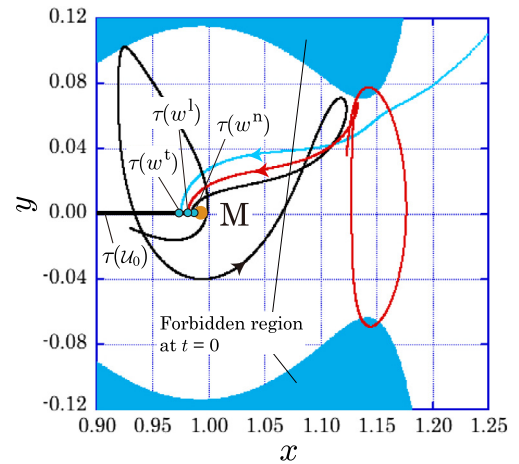


Fig. 14. Transit and non-transit orbits in the Sun-perturbed system.

as in Fig. 13, then the orbits in backward-time are transit and non-transit orbits respectively, as illustrated in Fig. 14. Hence it is clear that the LCS plays the role of separatrices in the Sun-perturbed system.

We also can compute the attracting LCS for the other cases of the instantaneous energy $E_{t_0}^{EM}$ at $t = t_0$.

5. Coupled 3-body system with perturbations and a low energy Earth–Moon transfer

In this section, we propose a design method of a low energy Earth–Moon transfer considering departure and arrival conditions in the framework of the coupled 3-body system with perturbations, referring to Onozaki et al. (2016a,b). Of course, there are numerous candidates of low energy transfers for the departure and arrival conditions, and the global study for optimal transfers is an interesting topic. However, we consider a particular case since our main purpose here is to show how to design such a low energy transfer for some given boundary conditions.

We leave the study of the global optimization to future work.

5.1. Family of departure trajectories in the Moon-perturbed system

In this paper, we consider the case in which the spacecraft is initially located in a LEO (167 km, 7.80713 km/s). Then, the spacecraft is transferred from the LEO into a departure trajectory by an impulsive maneuver with a change in velocity magnitude ΔV_E , where ΔV_E is produced in the direction parallel to the tangent velocity of the LEO, as in Fig. 15. The departure trajectory is chosen so that a non-transit orbit is outside the stable manifold $\bar{W}_{2,E}^s$ in the Moon-perturbed system. Otherwise, the spacecraft would move away from the vicinity of the Earth along a transit orbit. In this section, we construct the departure trajectories as a family of non-transit orbits.

We choose the celestial angle at the maneuver as $\bar{\theta}_M = 0$ rad, so the maneuver point on the LEO is set to

$$(\bar{x}, \bar{y}, \bar{v}_x, \bar{v}_y) = (1 - \mu_S - \alpha_M \mu_M - \bar{r}_{LEO}, 0, 0, -\bar{v}_{LEO} + \bar{r}_{LEO}) = (0.999922, 0, 0, -0.261750),$$

where $\bar{r}_{LEO} = 4.37038 \times 10^{-5}$ denotes the distance from the Earth's center to the spacecraft and $\bar{v}_{LEO} = 0.261408$ the velocity of the LEO in the Moon-perturbed system. The energy at the point can be obtained as $\bar{E}_{LEO}^{SE} = -1.53409$ by Eq. (3). The point \bar{w}_D after the maneuver is given by

$$(\bar{x}_D, \bar{y}_D, \bar{v}_{xD}, \bar{v}_{yD}) = (1 - \mu_S - \alpha_M \mu_M - \bar{r}_{LEO}, 0, 0, -\bar{v}_{LEO} + \bar{r}_{LEO} - \Delta V_E) = (0.999922, 0, 0, -0.261750 - \Delta V_E),$$

where the point \bar{w}_D is an initial point of the departure trajectory. Denote the energy at the point \bar{w}_D by $\bar{E}_{i_0}^{SE}$. Therefore, ΔV_E is uniquely obtained by the energy $\bar{E}_{i_0}^{SE}$.

Since we require the departure trajectory from the initial point \bar{w}_D to be a non-transit orbit, the point \bar{w}_D should be outside $\bar{W}_{2,E}^s$. Let us find the energy range, or the maneuver range, so that the point \bar{w}_D satisfies this condition. To do

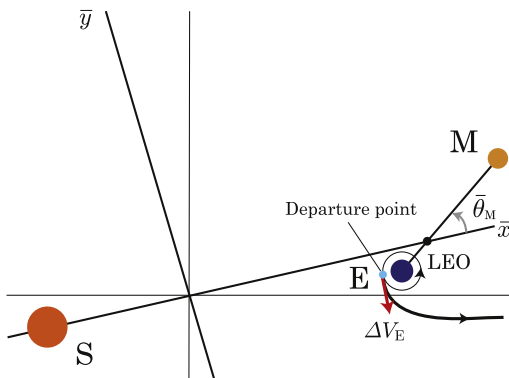


Fig. 15. Configuration of departure point.

this, we use the Poincaré section defined in Eq. (7) and investigate the stable manifold $\bar{W}_{2,E}^s$ on \bar{U} , as described in 4.3.

We show the stable manifold $\bar{\Gamma}_{2,E}^{1,s}$ in the case of $\bar{E}_{i_0}^{SE} = -1.50043$ in Fig. 16, which is the minimum energy for $\bar{\Gamma}_{2,E}^{1,s}$ to emerge in the FTLE field. The LEO and the patch point \bar{w}_D are also illustrated in Fig. 16. Since \bar{w}_D is outside $\bar{\Gamma}_{2,E}^{1,s}$, the lower limit of the energy is chosen as $\bar{E}_{D_{min}}^{SE} = -1.50043$. This energy leads to $\Delta V_E = 3.189$ km/s. In Fig. 17, we also show $\bar{\Gamma}_{2,E}^{1,s}$ in the case of $\bar{E}_{i_0}^{SE} = -1.50027$, which is the maximum energy such that \bar{w}_D is outside $\bar{\Gamma}_{2,E}^{1,s}$. Then, we can set the upper limit of the energy as $\bar{E}_{D_{max}}^{SE} = -1.50027$ ($\Delta V_E = 3.202$ km/s). Therefore, we can define the energy range as $\bar{E}_{D_{min}}^{SE} \leq \bar{E}_{i_0}^{SE} \leq \bar{E}_{D_{max}}^{SE}$.

In this way, we construct the family of departure trajectories parameterized by the energy $\bar{E}_{i_0}^{SE}$. Define the family of the departure trajectories by

$$\mathcal{D}(\bar{E}_{i_0}^{SE}) = \{ \phi_{i_0}^{\bar{}}(\bar{w}_D) \in TQ \mid \bar{w}_D \in \bar{\mathcal{E}}(\mu, \bar{E}_{i_0}^{SE}), \bar{E}_{i_0}^{SE} \in [\bar{E}_{D_{min}}^{SE}, \bar{E}_{D_{max}}^{SE}] \}.$$

Choosing 50 values for the energy $\bar{E}_{i_0}^{SE} \in [\bar{E}_{D_{min}}^{SE}, \bar{E}_{D_{max}}^{SE}]$, the family of the departure trajectories is obtain in Fig. 18.

5.2. Family of arrival trajectories in the Sun-perturbed system

Consider another boundary condition for the spacecraft; namely, we demand that the spacecraft is transferred from an arrival trajectory into a LLO (100 km, 1.63346 km/s) by a correction maneuver ΔV_M in the Sun-perturbed system. The arrival trajectory is required to be a transit orbit that is inside the unstable manifold $W_{2,M}^u$.

We set that the spacecraft arrives at

$$(x, y, v_x, v_y) = (1 - \mu_M - r_{LLO}, 0, 0, -v_{LLO} + r_{LLO}) = (0.983066, 0, 0, -1.58974),$$

where $r_{LLO} = 4.78018 \times 10^{-3}$ indicates the distance from the Moon's center to the spacecraft and $v_{LLO} = 1.59452$ the velocity of the spacecraft on the LLO in the Sun-perturbed system. In this paper, we choose the angle $\theta_M = 2.55$ rad on arrival, then the energy at the LLO point is $E_{LLO}^{EM} = -852.703$. We assume the correction maneuver is produced in the direction parallel to the tangent velocity of the LLO as in Fig. 19. Hence, the patch point w_A before the maneuver is obtained as

$$(x_A, y_A, v_{xA}, v_{yA}) = (1 - \mu_M - r_{LLO}, 0, 0, -v_{LLO} + r_{LLO} - \Delta V_M) = (0.983066, 0, 0, -1.58974 - \Delta V_M).$$

If we define the energy at w_A by $E_{i_0}^{EM}$, then we can uniquely determine the energy $E_{i_0}^{EM}$ associated with some correction maneuver ΔV_M . We will determine the energy range

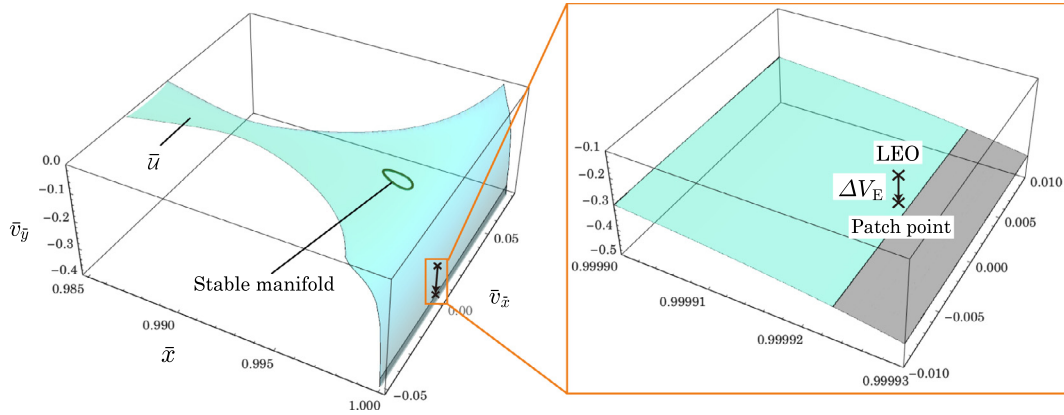


Fig. 16. Lower boundary of non-transit orbits ($\bar{E}_{t_0}^{SE} = -1.50043$).

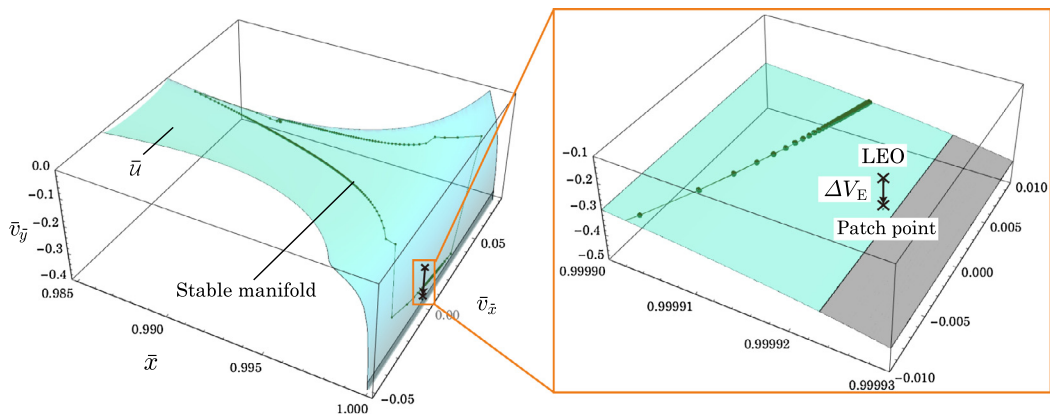


Fig. 17. Upper boundary of non-transit orbits ($\bar{E}_{t_0}^{SE} = -1.50027$).

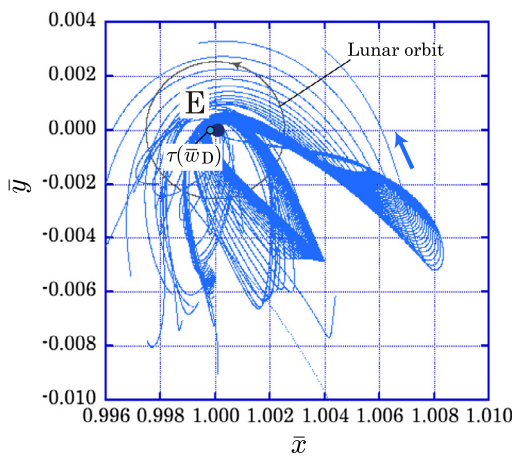


Fig. 18. Family of departure trajectories in the Moon-perturbed system ($\bar{E}_{t_0}^{SE} \in [\bar{E}_{D_{min}}^{SE}, \bar{E}_{D_{max}}^{SE}]$).

(associated with ΔV_M) so that the arrival trajectory is a transit orbit.

Therefore, the patch point w_A should be inside the unstable manifold $W_{2,M}^u$. To find a patch point that satisfies this condition, we investigate the unstable manifold $W_{2,M}^u$

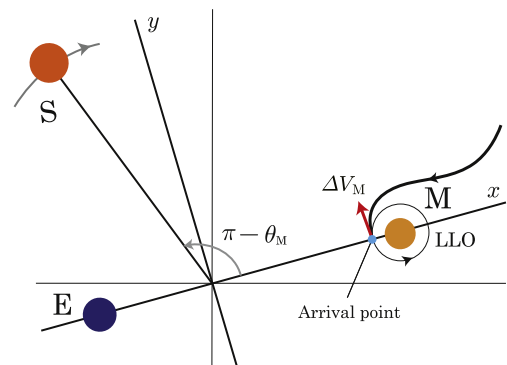


Fig. 19. Configuration of arrival point.

on the Poincaré section \mathcal{U} defined by Eq. (8). In Fig. 20, we illustrate the subset $\Gamma_{2,M}^{1,u}$ for the case of $E_{t_0}^{EM} = -851.528$ ($\Delta V_M = 0.634$ km/s), which is the minimum energy such that w_A is inside $\Gamma_{2,M}^{1,u}$. The patch point w_A and the LLO are also illustrated in Fig. 20. Therefore, we can determine the lower limit of the energy as $E_{A_{min}}^{EM} = -851.528$. Above the energy $E_{t_0}^{EM} = -851.528$, all arrival trajectories are considered to be transit orbits. Thus,

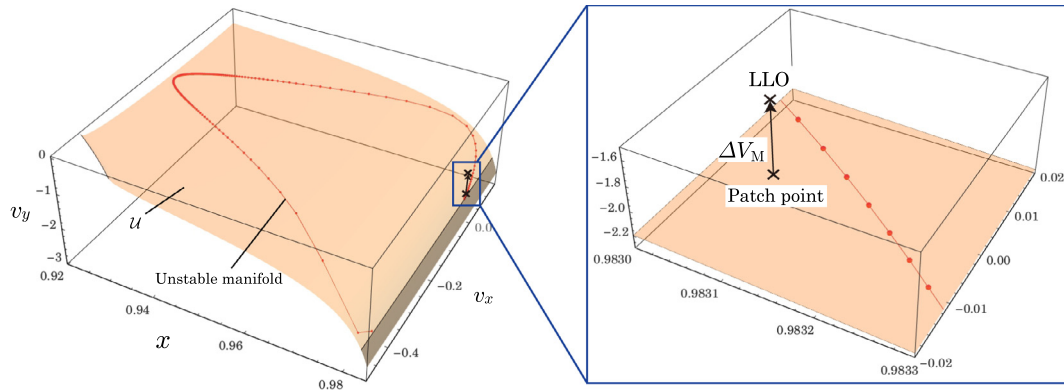


Fig. 20. Lower boundary of transit orbits ($E_{t_0}^{EM} = -851.528$).

the upper limit of the energy $E_{A_{max}}^{EM} = -851.493$ is determined by $\Delta V_M = 0.65$ km/s. The subset $\Gamma_{2,M}^{1,u}$ at $E_{t_0}^{EM} = -851.493$ is shown in Fig. 21. Hence, the energy range is obtained by $E_{A_{min}}^{EM} \leq E_{t_0}^{EM} \leq E_{A_{max}}^{EM}$.

Here, we use backward integration to construct the arrival trajectory that starts at the patch point w_A . The family of arrival trajectories is obtained by parameterizing the energy $E_{t_0}^{EM}$, which is given by

$$\mathcal{A}(E_{t_0}^{EM}) = \{ \phi_{t_0}^{-1}(w_A) \in TQ \mid w_A \in \mathcal{E}(\mu, E_{t_0}^{EM}), E_{t_0}^{EM} \in [E_{A_{min}}^{EM}, E_{A_{max}}^{EM}] \}.$$

In Fig. 22, we show the family of the arrival trajectories associated with 50 values of $E_{t_0}^{EM}$.

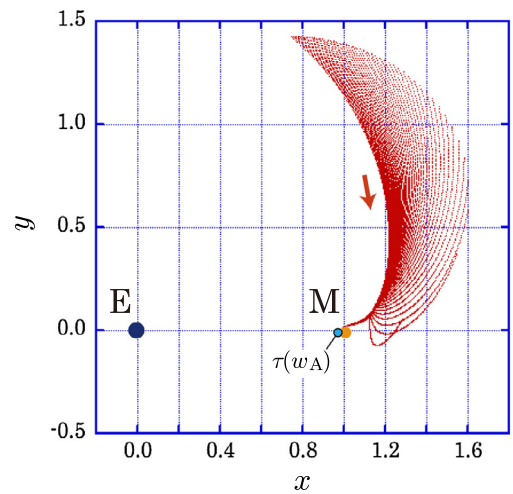


Fig. 22. Family of arrival trajectories in the Sun-perturbed system ($E_{t_0}^{EM} \in [E_{A_{min}}^{EM}, E_{A_{max}}^{EM}]$).

5.3. Design of low energy transfer from LEO to LLO

In this section, we show how to construct the transfer orbit from the LEO to the LLO. We choose one trajectory from the family of departure trajectories and one from the family of arrival trajectories, and we obtain the LEO–LLO transfer by patching two trajectories together with a maneuver ΔV_P .

Let us consider both families (i.e., the departure and arrival trajectories) in the same S–B_{EM} rotating frame in order to find appropriate trajectories. In Fig. 23, we show the family of arrival trajectories $\tilde{\varphi}(\mathcal{A}(E_{t_0}^{EM}))$ at $\bar{\theta}_M = 2.55$ rad in addition to the family of departure trajectories $\mathcal{D}(\bar{E}_{t_0}^{SE})$ at $\bar{\theta}_M = 0$ rad.

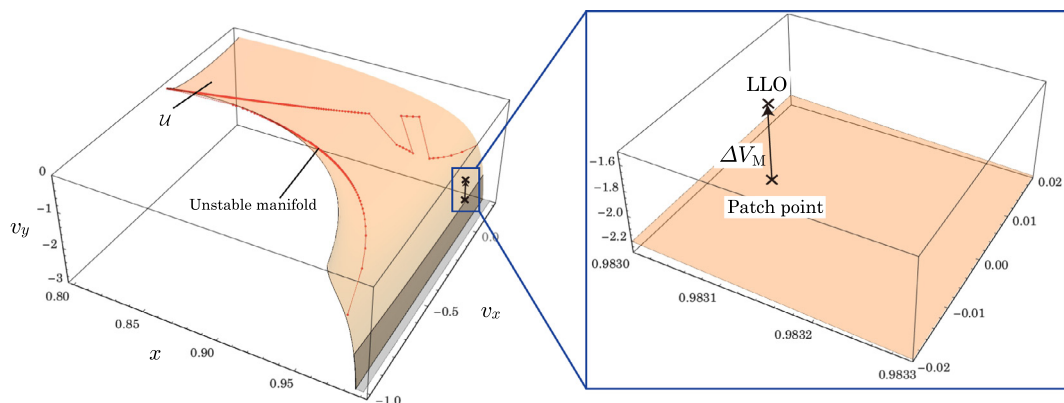


Fig. 21. Upper boundary of transit orbits ($E_{t_0}^{EM} = -851.493$).

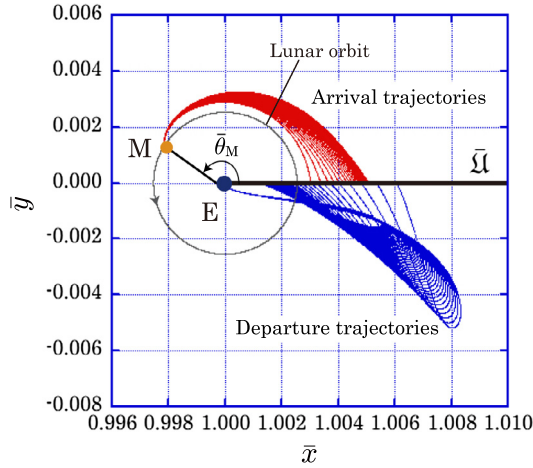


Fig. 23. Departure and arrival trajectories in the S-B_{EM} rotating coordinate.

Let $\tilde{w} = (\bar{x}, \bar{y}, \bar{v}_x, \bar{v}_y, \bar{\theta}_M) \in TQ \times S^1$ be a local coordinate in the extended space and let $\tilde{\pi} : TQ \times S^1 \rightarrow TQ$ be the projection map: $\tilde{\pi}(\tilde{w}) = \bar{w}$. To determine a patch point, set the Poincaré section on the \bar{x} axis as

$$\bar{U} = \{(\bar{x}, \bar{y}, \bar{v}_x, \bar{v}_y, \bar{\theta}_M) \in TQ \times S^1 \mid \bar{x} > 1 - \mu_S, \bar{y} = 0, \bar{v}_y > 0\}.$$

We show the family of departure trajectories crossing the section \bar{U} given by $\tilde{\pi}^{-1}(\mathcal{D}(\bar{E}_{t_0}^{SE})) \cap \bar{U}$ and the subset of the arrival trajectories $\tilde{\pi}^{-1}(\tilde{\varphi}(\mathcal{A}(E_{t_0}^{EM}))) \cap \bar{U}$. In Fig. 24, the subsets of departure trajectories are colored in blue and the arrival trajectories in red in $\bar{x}-\bar{\theta}_M-\bar{v}_x$ space. Fig. 25 illustrates the same subsets in $\bar{x}-\bar{\theta}_M-\bar{v}_y$ space. Define the patch points by

$$\tilde{w}^{SE} = (\bar{x}^{SE}, \bar{y}^{SE}, \bar{v}_x^{SE}, \bar{v}_y^{SE}, \bar{\theta}_M^{SE}) \in \tilde{\pi}^{-1}(\mathcal{D}(\bar{E}_{t_0}^{SE})) \cap \bar{U}$$

and

$$\tilde{w}^{EM} = (\bar{x}^{EM}, \bar{y}^{EM}, \bar{v}_x^{EM}, \bar{v}_y^{EM}, \bar{\theta}_M^{EM}) \in \tilde{\pi}^{-1}(\tilde{\varphi}(\mathcal{A}(E_{t_0}^{EM}))) \cap \bar{U}.$$

If we let $\tilde{\tau} : TQ \times S^1 \rightarrow Q \times S^1$, then the patch points are chosen so that $\tilde{\tau}(\tilde{w}^{SE}) = \tilde{\tau}(\tilde{w}^{EM}) : \bar{x}^{SE} = \bar{x}^{EM}, \bar{y}^{SE} = \bar{y}^{EM}$ and

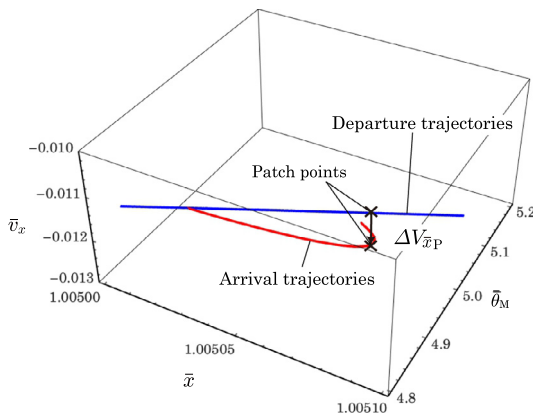


Fig. 24. Departure and arrival trajectories in $\bar{x}-\bar{\theta}_M-\bar{v}_x$ space.

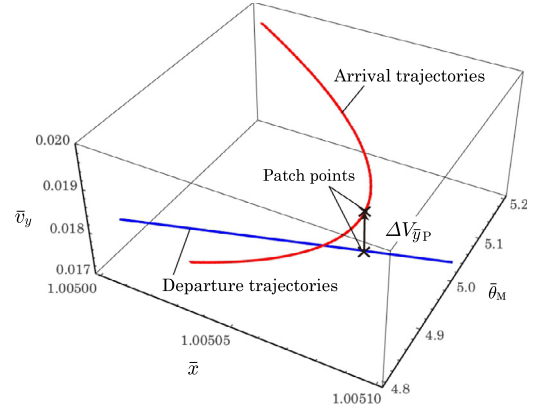


Fig. 25. Departure and arrival trajectories in $\bar{x}-\bar{\theta}_M-\bar{v}_y$ space.

$\bar{\theta}_M^{SE} = \bar{\theta}_M^{EM}$. Thus, the patch points are determined for the departure trajectory as

$$\begin{aligned} \tilde{w}^{SE} &= (\bar{x}^{SE}, \bar{y}^{SE}, \bar{v}_x^{SE}, \bar{v}_y^{SE}, \bar{\theta}_M^{SE}) \\ &= (1.00507, 0, -0.0113680, 0.0175449, 4.96074), \end{aligned}$$

and for the arrival trajectory as

$$\begin{aligned} \tilde{w}^{EM} &= (\bar{x}^{EM}, \bar{y}^{EM}, \bar{v}_x^{EM}, \bar{v}_y^{EM}, \bar{\theta}_M^{EM}) \\ &= (1.00507, 0, -0.0121205, 0.0184927, 4.96074). \end{aligned}$$

The maneuver to patch the departure and arrival trajectories is required as $\Delta V_P = 0.036$ km/s.

The departure trajectory can be computed from the initial point as

$$(\bar{x}_D, \bar{y}_D, \bar{v}_{xD}, \bar{v}_{yD}, \bar{\theta}_{MD}) = (0.999922, 0, 0, -0.368963, 0),$$

where the energy is $\bar{E}_{t_0}^{SE} = -1.50027$. It follows that $\Delta V_E = 3.202$ km/s. The final point of the arrival trajectory in the S-B_{EM} rotating frame is given by

$$(\bar{x}_A, \bar{y}_A, \bar{v}_{xA}, \bar{v}_{yA}, \bar{\theta}_{MA}) = (0.997900, 0.00140873, 0.0249961, 0.0372041, 2.55).$$

The energy of the arrival trajectory is $E_{t_0}^{EM} = -851.511$; hence, the maneuver is $\Delta V_M = 0.642$ km/s.

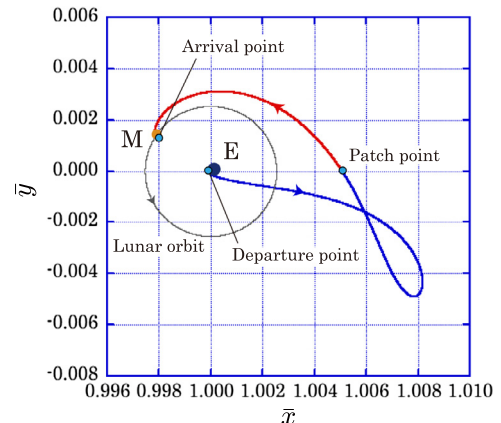


Fig. 26. Transfer from LEO to LLO in the S-B_{EM} rotating system.

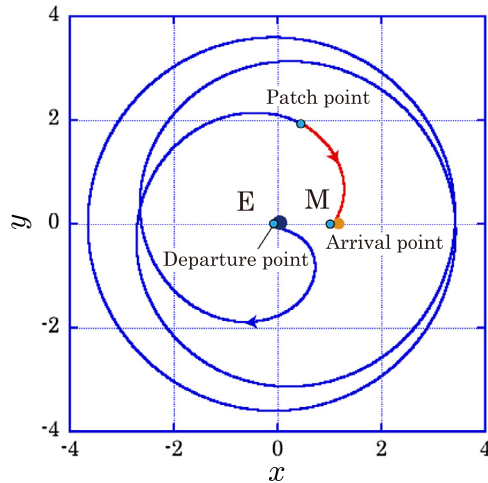


Fig. 27. Transfer from LEO to LLO in the E–M rotating system.

Table 1
Maneuver (ΔV [km/s]) and flight time (T [d]).

Transfer	ΔV_E	ΔV_M	ΔV_P	ΔV_T	T
Hohmann	3.141	0.838	–	3.979	5
WSB (Belbruno and Miller, 1993)	3.161	0.648	0.029	3.838	160
Proposed transfer	3.202	0.642	0.036	3.880	100

We illustrate the obtained transfer from LEO to LLO in the S–B_{EM} rotating frame in Fig. 26 and also that in the E–M rotating frame in Fig. 27. In this transfer, we require a total maneuver of $\Delta V_T = \Delta V_E + \Delta V_P + \Delta V_M = 3.880$ km/s and a flight time of $T = 100$ d.

Finally, we compare the proposed transfer with the Hohmann transfer and the WSB transfer of Belbruno and Miller (1993) in Table 1. We obtain the Hohmann transfer as the elliptic orbit connecting the LEO with the lunar orbit. As in Table 1, it follows that the total maneuver of the proposed approach is 0.099 km/s less than the Hohmann transfer though the flight time of our transfer is much greater than that of the Hohmann transfer. Comparing our transfer with the WSB transfer, the total maneuver is 0.042 km/s greater than that of the WSB, while the flight time is less by 60 d.

6. Conclusions

We have shown the design of a low energy transfer from the Earth to the Moon for the restricted 4-body system in the context of coupled 3-body system with perturbations. Specifically, we have regarded the Sun–Earth–Moon–S/C system as a coupled system of the Sun–Earth–S/C system perturbed by the Moon (the Moon-perturbed system) and the Earth–Moon–S/C system perturbed by the Sun (the Sun-perturbed system), and the coupling process has been made based on tube dynamics. The main advantage of this model is that one can apply the conventional method of the coupled 3-body problem to the coupled perturbed 3-body system. One can obtain the analogs of the

invariant manifolds of the perturbed 3-body system by using the technique of Lagrangian Coherent Structures (LCS), and one can also make use of their tube structures to design the low energy trajectories. To do this, we have computed the FTLE field to detect the LCS as second-derivative ridges by estimating the higher-order errors, and we have shown that the stable and unstable manifolds of the perturbed 3-body system separate orbits into transit and non-transit orbits as in a 3-body system. Furthermore, we have investigated the boundary conditions for designing a low energy transfer, in which the spacecraft departs from a LEO and arrives into a LLO and we have constructed families of departure and arrival trajectories. Finally, we have constructed a low energy transfer from the Earth to the Moon by patching together the departure and arrival trajectories, and the transfer required total maneuvers summing to 0.099 km/s less than in a comparative Hohmann transfer. In comparison with the WSB transfer, the proposed transfer leads to a significantly shorter flight time, albeit, a slightly higher maneuver cost of 0.043 km/s.

Acknowledgements

K.O. is partially supported by Waseda University (2016S–056, Grant-in-Aid for Young Scientists: Early Bird) and the MEXT “Top Global University Project” at Waseda University. H. Y. is partially supported by JSPS Grant-in-Aid for Scientific Research (26400408, 16KT0024, 24224004), Waseda University Grant for Special Research Project (2017K-167), and the MEXT “Top Global University Project” at Waseda University. S. D. R. is partially supported by the National Science Foundation under awards 1150456 and 1537349.

Appendix A. FTLE with estimation of truncation errors

Recall that the FTLE is computed from the state transition matrix, the elements of which may be approximated numerically by a central difference. The numerical error of the matrix could cause a significant error for the FTLE computations, in particular, near certain singular points. Here, we estimate the truncation errors for the state transition matrix and choose the matrix so that the truncation error can be sufficiently smaller than some value that we set. The round-off errors in the state transition matrix are not considered since the truncation errors dominate the round-off errors for the quadruple precision numbers in this study.

If we let $[\phi_{t_0}^{t_0+T}(w)]_i$ be the i th component of $\phi_{t_0}^{t_0+T}(w)$, then the state transition matrix is

$$\frac{d\phi_{t_0}^{t_0+T}(w)}{dw} = \begin{pmatrix} \frac{\partial[\phi_{t_0}^{t_0+T}(w)]_1}{\partial w_1} & \cdots & \frac{\partial[\phi_{t_0}^{t_0+T}(w)]_1}{\partial w_n} \\ \vdots & \ddots & \vdots \\ \frac{\partial[\phi_{t_0}^{t_0+T}(w)]_n}{\partial w_1} & \cdots & \frac{\partial[\phi_{t_0}^{t_0+T}(w)]_n}{\partial w_n} \end{pmatrix}.$$

The element $\frac{\partial[\phi_{t_0}^{t_0+T}(w)]_i}{\partial w_j}$ is approximated by a second-order central difference s_{ij} . If the central difference is given by a spatial discrete size Δw_j ,

$$s_{ij} = \frac{[\phi_{t_0}^{t_0+T}(w_1, \dots, w_j + \Delta w_j, \dots, w_n)]_i - [\phi_{t_0}^{t_0+T}(w_1, \dots, w_j - \Delta w_j, \dots, w_n)]_i}{2\Delta w_j},$$

then we can write

$$\frac{\partial[\phi_{t_0}^{t_0+T}(w)]_i}{\partial w_j} = s_{ij} - \frac{1}{6} \frac{\partial^3[\phi_{t_0}^{t_0+T}(w)]_i}{\partial w_j^3} \Delta w_j^2 + \mathcal{O}(\Delta w_j^4). \quad (\text{A.1})$$

Now, we approximate the element by the central difference \bar{s}_{ij} with another spatial discrete size $\bar{\Delta} w_j (< \Delta w_j)$,

$$\frac{\partial[\phi_{t_0}^{t_0+T}(w)]_i}{\partial w_j} = \bar{s}_{ij} - \frac{1}{6} \frac{\partial^3[\phi_{t_0}^{t_0+T}(w)]_i}{\partial w_j^3} \bar{\Delta} w_j^2 + \mathcal{O}(\bar{\Delta} w_j^4), \quad (\text{A.2})$$

where

$$\bar{s}_{ij} = \frac{[\phi_{t_0}^{t_0+T}(w_1, \dots, w_j + \bar{\Delta} w_j, \dots, w_n)]_i - [\phi_{t_0}^{t_0+T}(w_1, \dots, w_j - \bar{\Delta} w_j, \dots, w_n)]_i}{2\bar{\Delta} w_j}.$$

Thus, the truncation error $\bar{\epsilon}_{ij}$ is given by

$$\bar{\epsilon}_{ij} = -\frac{1}{6} \frac{\partial^3[\phi_{t_0}^{t_0+T}(w)]_i}{\partial w_j^3} \bar{\Delta} w_j^2 + \mathcal{O}(\bar{\Delta} w_j^4). \quad (\text{A.3})$$

We take the difference between Eqs. (A.1) and (A.2):

$$s_{ij} - \bar{s}_{ij} - \frac{1}{6} \frac{\partial^3[\phi_{t_0}^{t_0+T}(w)]_i}{\partial w_j^3} (\Delta w_j^2 - \bar{\Delta} w_j^2) + \mathcal{O}(\Delta w_j^4 - \bar{\Delta} w_j^4) = 0.$$

Ignoring the quartic and higher terms in the above equation, we obtain the following expression.

$$\frac{\partial^3[\phi_{t_0}^{t_0+T}(w)]_i}{\partial w_j^3} \approx \frac{6(s_{ij} - \bar{s}_{ij})}{(\Delta w_j^2 - \bar{\Delta} w_j^2)}. \quad (\text{A.4})$$

By inserting Eq. (A.4) into Eq. (A.3) and removing the quartic and higher terms, the truncation error is obtained as

$$\bar{\epsilon}_{ij} \approx (s_{ij} - \bar{s}_{ij}) \frac{\bar{\Delta} w_j^2}{(\Delta w_j^2 - \bar{\Delta} w_j^2)}.$$

In this paper, we assume that the discrete size is uniform for all elements, that is, $\bar{\Delta} w_i = \bar{\Delta} w_j$ ($i, j = 1, \dots, n$). We define an acceptable error by ϵ_{TOL} . If the truncation error is smaller than the acceptable error,

$$\max_{i,j} |\bar{\epsilon}_{ij}| < \epsilon_{TOL}, \quad (\text{A.5})$$

then we employ the central difference \bar{s}_{ij} in the computation of the FTLE. Otherwise we calculate the truncation error again by using a new smaller discrete size until Eq. (A.5) is satisfied.

References

Bate, R.R., Mueller, D.D., White, J.E., 1971. *Fundamentals of Astrodynamics*. Dover Publications, New York, p. 455.

- Belbruno, E.A., 1987. Lunar capture orbits, a method of constructing earth moon trajectories and the lunar GAS mission. In: 19th International Electric Propulsion Conference, p. 10.
- Belbruno, E.A., Miller, J.K., 1993. Sun-perturbed Earth-to-moon transfers with ballistic capture. *J. Guid. Control Dyn.* 16 (4), 770–775. <http://dx.doi.org/10.2514/3.21079>.
- Blazevski, D., Haller, G., 2014. Hyperbolic and elliptic transport barriers in three-dimensional unsteady flows. *Physica D*, 46–64. <http://dx.doi.org/10.1016/j.physd.2014.01.007>.
- Conley, C.C., 1968. Low energy transit orbits in the restricted three-body problem. *SIAM J. Appl. Math.* 16 (4), 732–746.
- Farazmand, M., Haller, G., 2012. Computing Lagrangian coherent structures from their variational theory. *Chaos* 22, 013128–1–013128–12. <http://dx.doi.org/10.1063/1.3690153>.
- Gawlik, E.S., Marsden, J.E., Du Toit, P.C., Campagnola, S., 2009. Lagrangian coherent structures in the planar elliptic restricted three-body problem. *Celest. Mech. Dyn. Astron.* 103 (3), 227–249. <http://dx.doi.org/10.1007/s10569-008-9180-3>.
- Haller, G., 2001. Distinguished material surfaces and coherent structures in three-dimensional fluid flows. *Physica D* 194 (4), 248–277. [http://dx.doi.org/10.1016/S0167-2789\(00\)00199-8](http://dx.doi.org/10.1016/S0167-2789(00)00199-8).
- Haller, G., 2011. A variational theory of hyperbolic Lagrangian Coherent Structures. *Physica D* 240 (7), 574–598. <http://dx.doi.org/10.1016/j.physd.2010.11.010>.
- Huang, S.S., 1960. Very restricted four-body problem, NASA Technical Note, D-501.
- Koon, W.S., Lo, M.W., Marsden, J.E., Ross, S.D., 2001. Low energy transfer to the Moon. *Celest. Mech. Dyn. Astron.* 81 (1), 63–73. <http://dx.doi.org/10.1023/A:1013359120468>.
- Koon, W.S., Lo, M.W., Marsden, J.E., Ross, S.D., 2011. *Dynamical Systems, the Three-Body Problem and Space Mission Design*, (Marsden Books), ISBN 978-0-615-24095-4.
- Mingotti, G., Toppato, F., Bernelli-Zazzera, F., 2009. Low-energy, low-thrust transfers to the Moon. *Celest. Mech. Dyn. Astron.* 105, 61–74. <http://dx.doi.org/10.1007/s10569-009-9220-7>.
- Onozaki, K., Yoshimura, H., 2014. Invariant manifolds and Lagrangian coherent structures in the planar circular restricted three-body problem. *Theoret. Appl. Mech. Jpn.* 62, 119–128. <http://dx.doi.org/10.11345/nctam.62.119>.
- Onozaki, K., Yoshimura, H., Ross, S.D., 2016a. Tube dynamics and low energy trajectory from the Earth to the Moon in the coupled three-body system. In: *Proceedings of 6th International Conference on Astrodynamics Tools and Techniques (ICATT)*, Darmstadt, Germany, 7p.
- Onozaki, K., Yoshimura, H., Ross, S.D., 2016b. The Earth-Moon low-energy transfer in the 4-body problem. In: *Proceedings of 26th AAS/AIAA Space Flight Mechanics Meeting*, Napa, California, AAS 16–405, 16p.
- Oshima, K., Yanao, T., 2014. Applications of gravity assists in the bicircular and bielliptic restricted four-body problem. In: *Proceedings of 24th AAS/AIAA Space Flight Mechanics Meeting*, Santa Fe, New Mexico, AAS 14–234, pp. 503–522.
- Parker, J.S., 2006. Families of low-energy lunar Halo transfers. *Advances in the Astronautical Sciences*, AAS 06–132, 20p.
- Parker, J.S., 2009. Low-energy ballistic transfers to lunar halo orbits. In: *Proceedings of 2009 AAS/AIAA Astrodynamics Specialist Conference*, Pittsburgh, Pennsylvania, AAS 09–443, p. 20.
- Pérez, D., Gómez, G., Masdemont, J.J., 2012. Detecting invariant manifolds using hyperbolic Lagrangian coherent structures. In: *Proceedings of the IAA/AAS Conference on the Dynamical Control of Space Systems*, Porto, Portugal, IAA-AAS Paper No. DyCoSS1 08–06, 13p.
- Pérez, D., Masdemont, J.J., Gómez, G., 2015. Tools to detect structures in dynamical systems using Jet Transport. *Celest. Mech. Dyn. Astron.* 123 (3), 239–262. <http://dx.doi.org/10.1007/s10569-015-9634-3>.
- Press, W., Teukolsky, S., Vetterling, W., Flannery, B., 1992. *Numerical Recipes in Fortran 77: The Art of Scientific Computing*. Cambridge University Press, p. 933.

- Qi, R., Xu, S., Zhang, Y., Wang, Y., 2012. Earth-to-Moon low energy transfer using time-dependent invariant manifolds. In: AIAA/AAS Astrodynamics Specialist Conference, Minneapolis, Minnesota, AIAA 2012-443, pp. 1–11.
- Ross, S.D., Tanaka, M.L., Senatore, C., 2010. Detecting dynamical boundaries from kinematic data in biomechanics. *Chaos: Interdiscip. J. Nonlinear Sci.* 20 (017507), 13. <http://dx.doi.org/10.1063/1.3267043>.
- Shadden, S.C., Lekien, F., Marsden, J.E., 2005. Definition and properties of Lagrangian coherent structures from finite-time Lyapunov exponents in two-dimensional aperiodic flows. *Physica D* 212 (3–4), 271–304. <http://dx.doi.org/10.1016/j.physd.2005.10.007>.
- Short, C.R., Howell, K.C., 2014. Lagrangian coherent structures in various map representations for application to multi-body gravitational regimes. *Acta Astronaut.* 94 (2), 592–607. <http://dx.doi.org/10.1016/j.actaastro.2013.08.020>.
- Short, C.R., Blazevski, D., Howell, K.C., Haller, G., 2015. Stretching in phase space and applications in general nonautonomous multi-body problems. *Celest. Mech. Dyn. Astron.* 122 (3), 213–238. <http://dx.doi.org/10.1007/s10569-015-9617-4>.
- Simó, C., Gómez, G., Jorba, Á., Masdemont, J., 1995. The bicircular model near the triangular libration points of the RTBP. *From Newton to Chaos* 336, 343–370.
- Szebehely, V., 1967. *Theory of Orbits: The Restricted Problem of Three Bodies*. Academic Press, New York.
- Tallapragada, P., Ross, S.D., 2008. Particle segregation by Stokes number for small neutrally buoyant spheres in a fluid. *Phys. Rev. E* 78 (3), 9. <http://dx.doi.org/10.1103/PhysRevE.78.036308>, No. 036308.
- Tallapragada, P., Ross, S.D., 2013. A set oriented definition of finite-time Lyapunov exponents and coherent sets. *Commun. Nonlinear Sci. Numer. Simul.* 18 (5), 1106–1126. <http://dx.doi.org/10.1016/j.cnsns.2012.09.017>.
- Topputo, F., 2013. On optimal two-impulse Earth-Moon transfers in a four-body model. *Celest. Mech. Dyn. Astron.* 117 (3), 279–313. <http://dx.doi.org/10.1007/s10569-013-9513-8>.